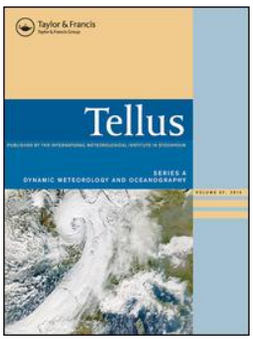

Tellus A: Dynamic Meteorology and Oceanography

ISSN: (Print) 1600-0870 (Online) Journal homepage: https://www.tandfonline.com/loi/zela20

Environmental conditions for polar low formation and development over the Nordic Seas: study of January cases based on the Arctic System Reanalysis

Ana Radovan, Susanne Crewell, Erlend Moster Knudsen & Annette Rinke

To cite this article: Ana Radovan, Susanne Crewell, Erlend Moster Knudsen & Annette Rinke (2019) Environmental conditions for polar low formation and development over the Nordic Seas: study of January cases based on the Arctic System Reanalysis, Tellus A: Dynamic Meteorology and Oceanography, 71:1, 1-16, DOI: 10.1080/16000870.2019.1618131

To link to this article: https://doi.org/10.1080/16000870.2019.1618131

Published online: 05 Jun 2019.

Tellus SERIES A DYANAMIC METEOROLOGY AND OCEANOGRAPHY
PUBLISHED BY THE INTERNATIONAL METEOROLOGICAL INSTITUTE IN STOCKHOLM

Environmental conditions for polar low formation and development over the Nordic Seas: study of January cases based on the Arctic System Reanalysis

By ANA RADOVAN[1]*, SUSANNE CREWELL[1], ERLEND MOSTER KNUDSEN[1†], and ANNETTE RINKE[2], [1]*Institute of Geophysics and Meteorology, University of Cologne, Cologne, Germany;* [2]*Alfred Wegener Institute, Helmholtz Centre for Polar and Marine Research, Potsdam, Germany*

(Manuscript received 04 December 2018; in final form 06 May 2019)

ABSTRACT

The sparse observational network over the Arctic region makes severe storms such as polar lows (PLs) still hard to predict. To improve their forecasting and detection, it is of great importance to gain better understanding of their formation and development. Therefore, we have analyzed the environment of PLs at their genesis and mature stages using a set of parameters: the difference between sea surface and 500 hPa temperature (or at 2 m height), lapse rate (LR) and relative humidity below 850 hPa (RH), near-surface wind speed and geopotential height anomaly. We evaluate which of these conditions (or which combination) is(are) the most favourable for PL formation and persistence. The analysis was performed on 33 January cases over 12 years (2000–2011) using the Arctic System Reanalysis. The results showed that, for the cases with lower thermal instability during formation stage, LRs throughout the boundary layer were stronger and steeper; therefore, these PLs were fostering convective development. However, for few cases, it was noted that when convection decreased simultaneously with increased thermal stability, RH most of the times was above 90%. It was also noted that the higher amount of RH at lower levels during genesis stage promoted stronger winds at the maturity stage.

Keywords: mesoscale cyclone; polar low formation/ development; environmental conditions

1. Introduction

Throughout history, in the Arctic region, severe sudden storms that pose a great threat was well known to the coastal community. A sudden change of weather with a storm that brings heavy precipitation and strong winds causes substantial infrastructural damage, wreaks havoc on ships and disrupts shipping routes. Today, in a rapidly changing climate where the increase in near-surface air temperature in the Arctic region is twice the global value; term known as the Arctic amplification (Serreze and Francis, 2006), thinner sea ice is becoming more vulnerable to storms (Zabolotskikh et al., 2015). To understand the major feedback mechanisms of Arctic amplification, major efforts are being made to identify, investigate and evaluate the key processes that contribute to it (Wendisch et al., 2017). A study by Condron and Renfrew (2013) found that the most intense cyclones extract huge amounts of heat from the ocean ($\geq 1000\,\mathrm{Wm^{-2}}$) and thus affect open-ocean deep convection and subsequently the Atlantic meridional overturning circulation. Therefore, how these cyclones will occur and strengthen in the future climate is highly important, especially in the region of the Nordic Seas, which is already experiencing drastic changes (Carmack et al., 1997; Morison et al., 2012; Lind et al., 2018).

The first attempt to explain the formation of these severe storms was given by Dannevig (1954), where he referred to them as 'Arctic instability lows'. He noted that such a storm can develop due to instability within a cold air outbreak (CAO) that flows over the warmer sea. These severe storms were termed polar lows (PLs) (Harley, 1960) since they appear only over polar regions. The commonly used definition for this term has been proposed by Rasmussen and Turner (2003):

Polar low is a small, but fairly intense maritime cyclone that forms poleward of the main baroclinic zone (the polar front or other major baroclinic zone). The horizontal

*Corresponding author. e-mail: aradovan@uni-koeln.de
†Additional affiliation: StormGeo, Nordre Nøstekaien 15011 Bergen, Norway

Citation: Tellus A: 2019, **71**, 1618131, https://doi.org/10.1080/16000870.2019.1618131

scale of polar low is approximately between 200 and 1000 km and surface winds near or above gale force.

However, as the observational network over the Arctic Ocean is sparse and PLs are relatively small and short-lived maritime cyclones (can last only 4 h (Blechschmidt, 2008)), their prediction still presents a challenge. Improving their treatment in numerical models requires a deeper knowledge of the environmental conditions in which they form and develop.

Among the first theories that tried to explain the formation of a PL was the thermal instability theory, which proposes instability inside a CAO flowing over the warmer sea as the main mechanism (Dannevig, 1954). Although thermal instability partly explains the formation of PLs, this theory lacks the explaining mechanism for vorticity formation. The baroclinic instability theory was proposed by Harold and Browning (1969) showed that a low-level baroclinic field is necessary but is not sufficient for PL formation. Due to PLs' resemblance to tropical hurricanes on the satellite images, such as the frequently visible eye and the presence of spiral of cumulus clouds around it, convection was believed to explain their formation. Therefore, the conditional instability of the second kind (CISK) was proposed to account for PL genesis (Rasmussen, 1979). However, that mechanism was only able to explain the intensification of an already developed circulation (Charney and Eliassen, 1964; Sardie and Warner, 1983), and the calculated growth rates were too small. Another theory originating from the resemblance of PLs to tropical hurricanes is the Air–Sea Interaction Instability (ASII) theory was given by Emanuel (1986) and later renamed as the Wind-induced Surface Heat Exchange (WISHE) theory (Emanuel and Rotunno, 1989). According to that theory, a PL acquires energy from the sea surface fluxes and moist enthalpy, as also shown by Rasmussen (1979). However, the theory neglects environmental baroclinicity and is not able to produce the PL growth rate (Montgomery and Farrell, 1992). Sardie and Warner (1983) also showed that some PLs tend to be mainly baroclinic while others show strong convective features.

Despite the multitude of these theories about PL development, and despite several research aircraft campaigns into the topic (Shapiro et al., 1987; Douglas et al., 1995; Føre et al., 2011), the phenomena of PLs remain too complex to be explained by only one of the theories.

This difficulty has led to the acceptance of several mechanisms acting simultaneously in triggering and intensifying a PL and a spectrum between the extremely baroclinic and convective cases (Bracegirdle and Gray, 2008).

Our study improves understanding of PL formation and development by investigating a comprehensive set of parameters suggested in the literature for characterizing the environmental conditions. The study looked at different thresholds in these parameters to identify the most relevant one(s) or the most relevant combination. Furthermore, the parameters for both the genesis and maturity stage of PLs were investigated to potentially derive information on their development and persistence.

For this analysis, we used both versions of the Arctic System Reanalysis (ASR), which improves the depiction of mesoscale processes in the Arctic region (Bromwich et al., 2010, 2016). We focused on PL cases for January between 2000 and 2011 over the North Atlantic region. Generally, January is the month with highest PL occurrence (Noer et al., 2011) and also the coldest month of the PL season (October–May). The detailed description of the analysis technique and the set of parameters including their thresholds (from now on called conditions) are explained in Section 2. In Section 3, we present our results with two main focuses: first, the analysis of the parameters and their change from the genesis to maturity stage; second, the climatological perspective, where we compared the large-scale environment during PL genesis with the overall January climatology. In Section 4, we briefly discuss and conclude our results.

2. Data and methods

2.1. PL cases

The investigated January PL cases are based on the Noer and Lien (2010) list (hereinafter referred to as NL list). The NL list contains the date, time and coordinates of each PL case at its maturity stage. The stage of maturity is defined by inspecting advanced very high-resolution radiometer images, where a PL is noted as fully developed when the cloud band structure and a partially clear eye of the low is visible. In addition, whenever possible, wind speed, and gust information from the advanced scatterometer were registered. Using sea-level pressure analysis from the numerical weather prediction model High-Resolution Limited Area Model (HIRLAM) at 4 km resolution, minimum mean sea-level pressure (MSLP) was also recorded. For the 2000–2011 period, in total, 33 January cases were reported (Fig. 1).

2.2. ASR

The first version of ASR (ASRv1) is a 3-hour regional reanalysis with a horizontal resolution of $\sim$ 30 km and 29 pressure levels available for the 2000–2012 period. It is produced using the state-of-the-art Weather Research and Forecasting (WRF) Model tuned for polar regions (Bromwich et al., 2010). When compared to observations, the WRF showed good performance for surface variables

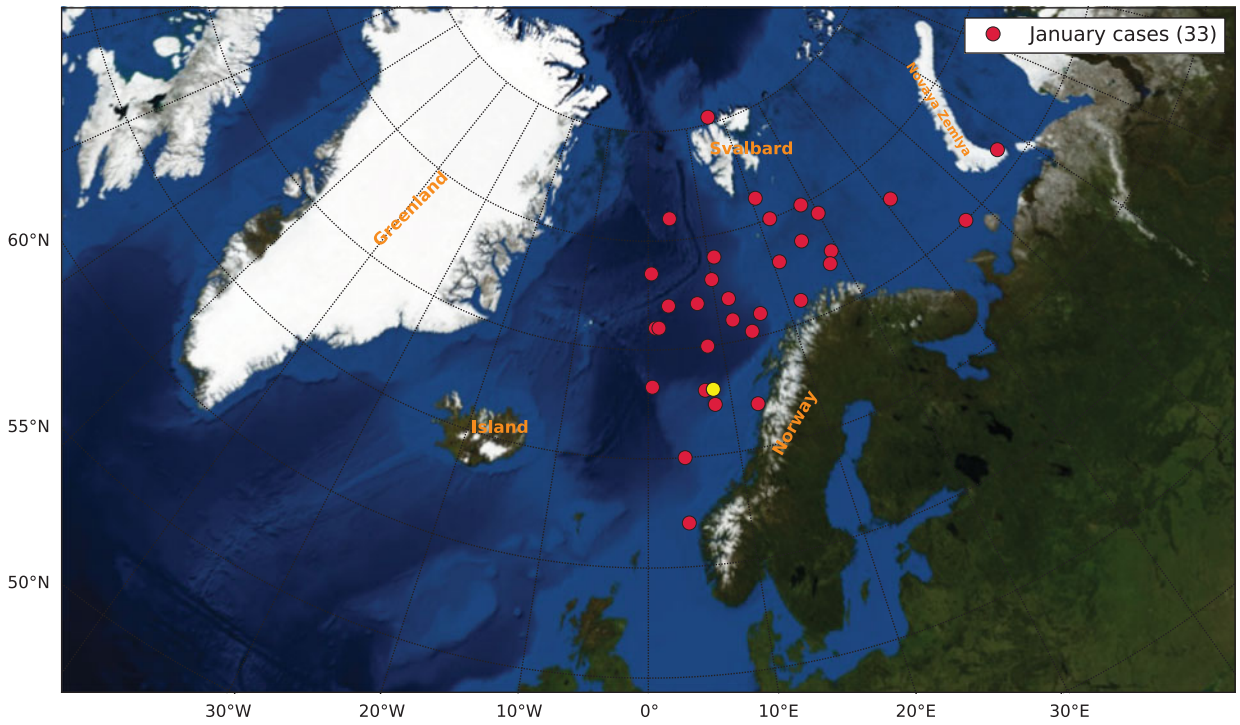

Fig. 1. January PLs between 2000 and 2011. Each of the 33 cases is represented at the location reported in the Noer and Lien (2010) list (red dots). The case marked with yellow is the one presented in Fig. 2.

with MSLP having the best prediction, while poorest performance is shown for near-surface wind speed due to inadequate modelling of local wind effects and obstructions (Bromwich et al., 2010). When compared to ECMWF Re-Analysis Interim (ERA-I), which has coarser temporal (6 hourly) and horizontal resolutions (~ 79 km), ASRv1 has improved modelling of near-surface wind fields and moisture while the remaining variables showed a similar behaviour (Wilson et al., 2011, 2012).

In addition, we also used the second version of ASR (ASRv2), which in comparison to ASRv1 has twice the horizontal resolution (15 km) and five more vertical levels (in total 34 levels). Besides resolution, it also has improvements in the model physics, including sub-grid scale cloud fraction interaction with radiation, and in the data assimilation scheme. This new version also shows improvements in reproduction of near-surface and tropospheric variables (Bromwich et al., 2018). Although ASRv2 is offered for a longer time span, 2000–2016, to compare our results to ASRv1, we have used data for the same period for which the ASRv1 was released. Moreover, 2012 was excluded from the analysis since there were no PLs in January that year.

Since PLs are 'extreme' maritime cyclones, it is of significance to check for ASR performance in respect to its general cyclones representation first. This has been done by Tilinina et al. (2014). They showed that the ASRv1, during winter, detects 28% more cyclones than ERA-I. A similar result was shown in Akperov et al., (2018), where it was found that ASRv2 resolves more small and shallow cyclones. Compared to the Noer et al. (2011) PL climatology, ASRv1 was able to resolve 89% of the PLs compared to 48% resolved in the ERA-I. ASRv1 also showed more realistic wind speed information that is closer to satellite observations (Smirnova and Golubking, 2017). In studies using ERA-I, Michel et al. (2018) and Zappa et al. (2014), the PL detections were 60% and 55% of those reported in the Sea Surface Temperature and Altimeter Synergy for Improved Forecasting of Polar Lows (STARS) data base (Ø.Saetra et al. 2010), respectively. Since ASRv1 proved to be more reliable in those studies, the choice of using ASR over ERA-I is justified.

2.3. PL genesis and maturity states

Investigating the environmental conditions (detailed in Section 2.4) at two different stages requires a time reference of a PL event. The maturity information was taken from the NL list, which notes the time of the maturity. Accordingly, we extracted the parameters from the ASR at the time step closest to maturity time. To analyze the

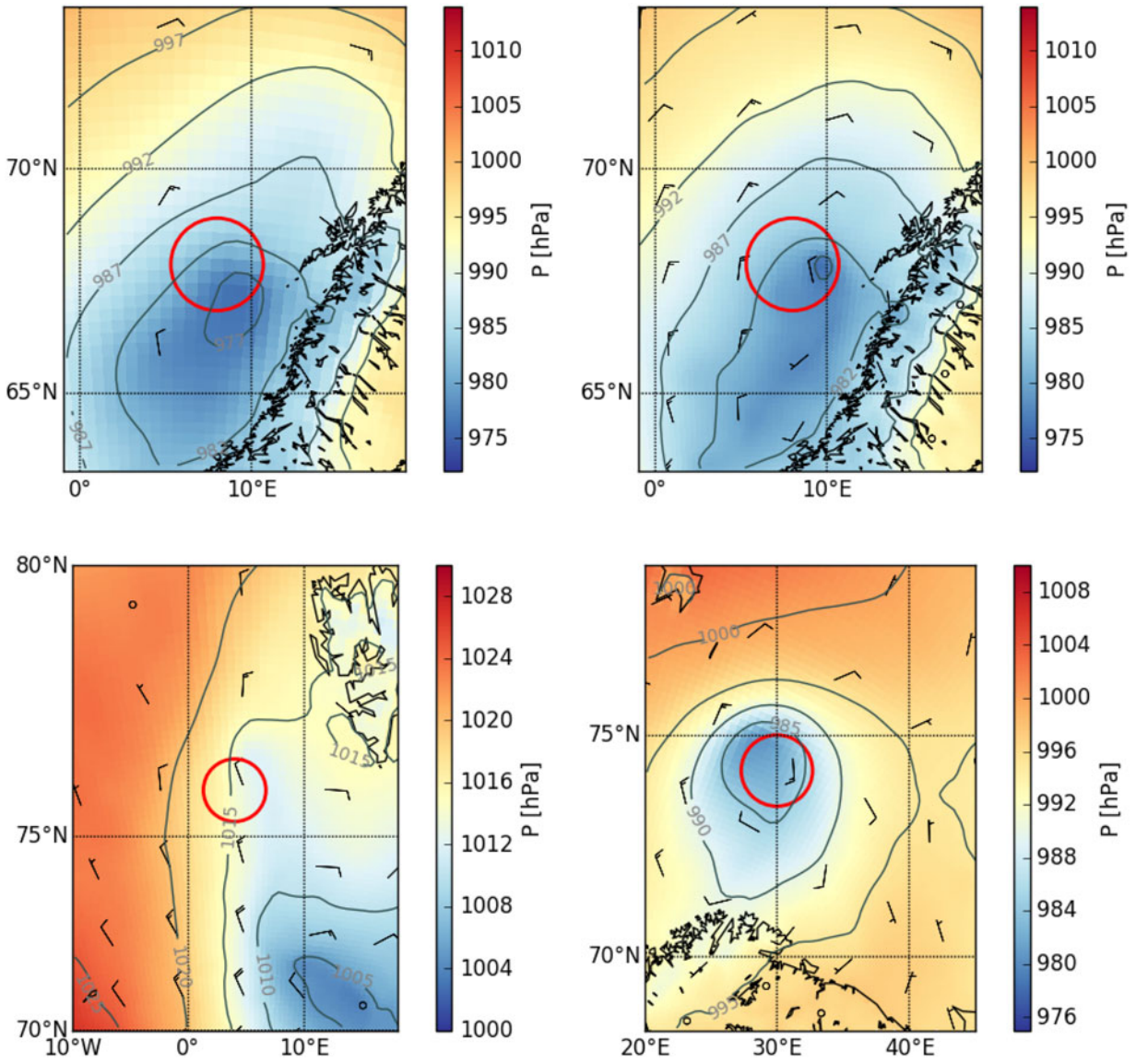

Fig. 2. MSLP (colour shading and grey counters every 5 hPa) and wind speed and direction (wind barbs) for PL cases on 29 January 2010 from ASRv1 (upper left) and ASRv2 (upper right) and for 22 January 2007 (lower left) and 30 January 2011 (lower right). Both cases in the bottom row were plotted using the ASRv2 data. The red circle indicates a 200 km radius around the location from NL list.

same environmental conditions at the genesis stage, we were followed the procedure by Terpstra et al. (2016) and took the genesis time to be 6–9 h prior to the maturity time. This time interval was chosen to take into account the time needed for PL development and the 3-hour resolution of the ASR.

At the genesis time, for each case, an area in the 200 km radius around the genesis point was used for the analysis. The small scale of PLs and the fact that only 2% of the polar mesocyclones identified on satellite imagery have a diameter less than 200 km supports usage of that area as representative of the pre-PL environment (Condron et al., 2006). Due to this assumption, there could be larger spread of values in conditions in between cases. This can also, at times, attribute to different values of conditions in between reanalyses versions (Fig. 2 (top)). Moreover, the final value can also be affected by the lower precision of the PL location found in ASR when compared to the one noted in the NL list (Fig. 2 (bottom)) as well as due to a potential movement of the developed PL.

For the maturity stage, we checked which conditions were above the threshold of interest, when the PL was listed in NL, although the C1 condition (commonly used for detection) was not fulfilled. We aim to clarify by this the importance of the other conditions at the maturity state.

Table 1. PL conditions (denoted by C1,C2, … C6; see Section 2.4) and their values taken from various studies (second and third column, respectively). The last two columns give the 75 percentile means of C1, C2, C3, C4(i), C4(ii), maximum of C5 and mean of C6 for all the 33 cases during the genesis stage found using the ASR versions 1 and 2.

	Condition	Value	Source	ASRv1	ASRv2
C1	SST - T(500 hPa)	$\geq$ 43 K	Noer and Ovhed (2003)	46 K	45 K
C2	SST - T(2m)	$\sim$ 6 K	Terpstra et al. (2016)	6 K	8 K
C3	LR	cond. unstable below 850 hPa	Terpstra et al. (2016)	1.4 K/km	2.6 K/km
C4	(i) RH(surf.–950 hPa)	$\sim$ 75%	Terpstra et al. (2016)	80%	87%
	(ii) RH(950–850 hPa)	$\sim$ 82%	Terpstra et al. (2016)	91%	90%
C5	NSWS	$\geq$ 15 m s^{-1}	Rasmussen and Turner (2003)	16.2 m/s	17.6 m/s
C6	GPH anomaly	160 gpm	Forbes and Lottes (1985)	182 gpm	140 gpm

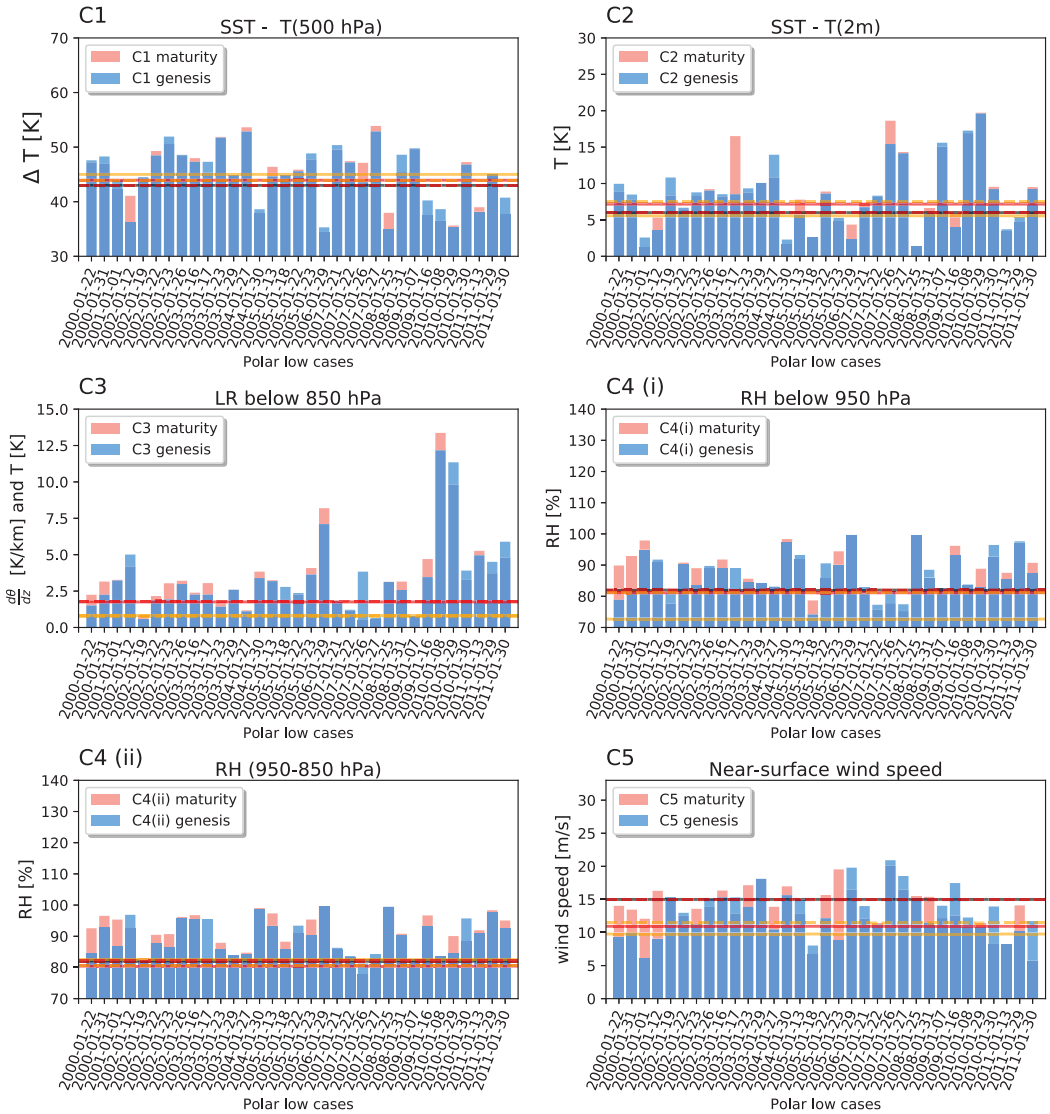

Fig. 3. Bars represent the values for the different conditions based on ASRv2 grid points within a 200 km radius around the genesis (blue) and maturity (orange) point for each of the January cases between 2000 and 2011. C1 (upper left), C2 (upper right), C3 (middle left), C4(i) (middle right), C4(ii) (bottom left) and C5 (bottom right). Horizontal lines represent: the literature threshold from Table 1 (black), ASRv2 mean (red) and ASRv1 mean (yellow) for genesis (maturity) stage denoted with full (dashed) line.

Table 2. Overview of conditions for each PL case at genesis stage with their dates and location. Values in the table are means for a 200 km radius around the genesis point.

	case	Coord.	C1 (K)	C2 (K)	C3 (K/km)	C4(ii) (%)	C5 (m/s)	C6 (m)	shear
1.	2000-01-22	72.5°N 29°E	47.6 ↓	10 ↓	0.62 ↑	85 ↑	11.97 ↑	- 144 ↓	R
2.	2000-01-31	65°N 4°E	48.3 ↓	8.5 ↓	1.47 ↑	93 ↑	17.2 ↑	- 282 ↑	R
3.	2001-01-01	75°N 22°E	43.9 ↓	2.6 ↓	2.93 ↑	87 ↑	12.8 ↑	- 44 ↑	R
4.	2002-01-12	73°N 21°E	36.2 ↑	3.6 ↑	3.51 ↓	97 ↓	16 ↑	- 56 ↓	-
5.	2002-01-19	70°N 47°E	44.5 ↓	10.8 ↓	0.48 ↑	82 ↑	18.7 ↓	- 292 ↑	-
6.	2002-01-22	75°N 28°E	48.5 ↑	6.7 ↓	1.76 ↑	88 ↑	22.6 ↓	- 207 ↑	R
7.	2002-01-23	71°N 16°E	51.9 ↓	8.8 ↓	1.78 ↑	86 ↑	19.4 ↑	- 281 ↓	R
8.	2002-01-26	72°N 12°E	48.6 ↓	9 ↑	1.91 ↓	96 ↑	19.7 ↓	- 187 ↓	R
9.	2003-01-16	72°N 7.3°E	47.3 ↑	8.5 ↓	2.08 ↑	95 ↑	22.2 ↑	- 259 ↑	R
10.	2003-01-17	73.5°N 25.5°E	47.3 ↓	8.5 ↑	1.22 ↓	95 ↓	22.2 ↓	- 259 ↓	R
11.	2003-01-23	73°N 10°E	51.7 ↑	9.3 ↓	2.08 ↑	86 ↑	18.5 ↑	- 262 ↑	R
12.	2003-01-29	73.5°N 0.5°E	44.7 -	10.1 -	1.23 -	84 -	19.8 -	- 98 -	-
13.	2004-01-27	71°N 12°E	52.9 ↑	14 ↓	1 ↑	84 ↑	17.3 ↑	- 271 ↑	R
14.	2004-01-30	70°N 8°W	38.6 ↓	2.3 ↓	3.5 ↑	99 ↑	17.7 ↑	- 201 ↑	R
15.	2005-01-13	68°N 7°E	44.6 ↑	5.7 ↑	3.01 ↓	93 ↑	19.4 ↓	- 50 ↑	-
16.	2005-01-18	72°N 3°W	44.8 ↑	2.6 ↓	0.22 ↑	86 ↑	11.4 ↓	- 203 ↑	R
17.	2005-01-22	66°N 6.3°E	45.6 ↑	8.6 ↑	2.16 ↓	93 ↓	15.7 ↑	- 90 ↑	-
18.	2005-01-23	67°N 13°E	48.8 ↓	5.3 ↓	3.24 ↑	90 ↑	20 ↑	- 120 ↑	-
19.	2006-01-29	Hopen	35.3 ↓	2.3 ↑	6.44 ↑	100 -	22.1 ↓	165 ↑	R
20	2007-01-21	73°N 41°E	50.4 ↓	6.7 ↑	1.74 ↓	86 ↓	16.4 ↓	- 149 ↑	R
21.	2007-01-22	76°N 4°E	47.2 ↑	8.3 ↓	0.91 ↓	84 ↓	15.2 ↑	- 184 ↑	R
22.	2007-01-26	70.3°N 14.3°E	43.6 ↑	15.4 ↑	0.51 ↓	81 ↓	22.1 ↓	- 256 ↓	-
23.	2007-01-27	71°N 22°E	52.9 ↑	14.2 ↑	0.63 ↓	84 ↓	20.1 ↓	- 304 ↓	R
24.	2008-01-25	67.3°N 8°E	48.6 ↑	1.4 ↓	2.55 ↑	99 ↓	17.9 ↑	- 67 ↓	-
25.	2008-01-31	74°N 11°E	35 ↓	6 ↑	2.48 ↑	90 ↑	13.9 ↑	- 137 ↓	R
26.	2009-01-07	72°N 28°E	49.8 ↓	15.6 ↓	0.6 ↓	83 ↑	19.5 ↓	- 232 ↑	-
27.	2009-01-16	71°N 57°E	40.2 ↓	3.9 ↑	3.1 ↑	93 ↑	19.7 ↓	88 ↑	-
28.	2010-01-08	80.3°N 16.3°E	38.6 ↓	17.3 ↓	9.7 ↑	84 ↓	15.4 ↓	82 ↑	R
29.	2010-01-29	68°N 8°E	35.4 ↑	19.6 ↑	10.66 ↓	85 ↑	14.9 ↑	74 ↓	R
30.	2010-01-30	62°N 4°E	46.8 ↑	9.2 ↑	2.97 ↓	96 ↓	16.6 ↓	- 191 ↑	F
31.	2011-01-13	71°N 1°W	38.2 ↑	3.7 ↓	4.64 ↑	91 ↑	15.5 ↑	- 56 ↑	-
32.	2011-01-29	71°N 1°W	45.1 ↓	5.4 ↓	3.84 ↓	98↑	14.5 ↑	- 99 ↓	-
33.	2011-01-30	74.3°N 30°E	40.7 ↓	9.2 ↑	2.05 ↑	93 ↑	14.7 ↓	- 70 ↑	-
ASRv2		**Mean**	45	8.2	2.64	89	17.6	- 141	
		Std	5.2	4.5	2.33	5	3.0	120	
ASRv1		**Mean**	46.2	6.5	1.47	91	16.3	-182	
		std	3.6	3.6	1.21	5	4.0	85	

Thresholds are marked in colours and, for the conditions C1–C5, have the following meaning: red – condition has not been fulfilled, yellow – condition is neutral (between one STD and the mean (or the threshold)) and green – condition is fulfilled. For C6, the colours indicate the following: red – conditions is above zero, yellow - condition is between zero and -160 gpm and green - condition is fulfilled. For the thresholds, refer to Table 1. The last two rows give the mean and STD of the condition of the respective column. The arrow next to each value represents an increase (decrease) at the maturity stage.

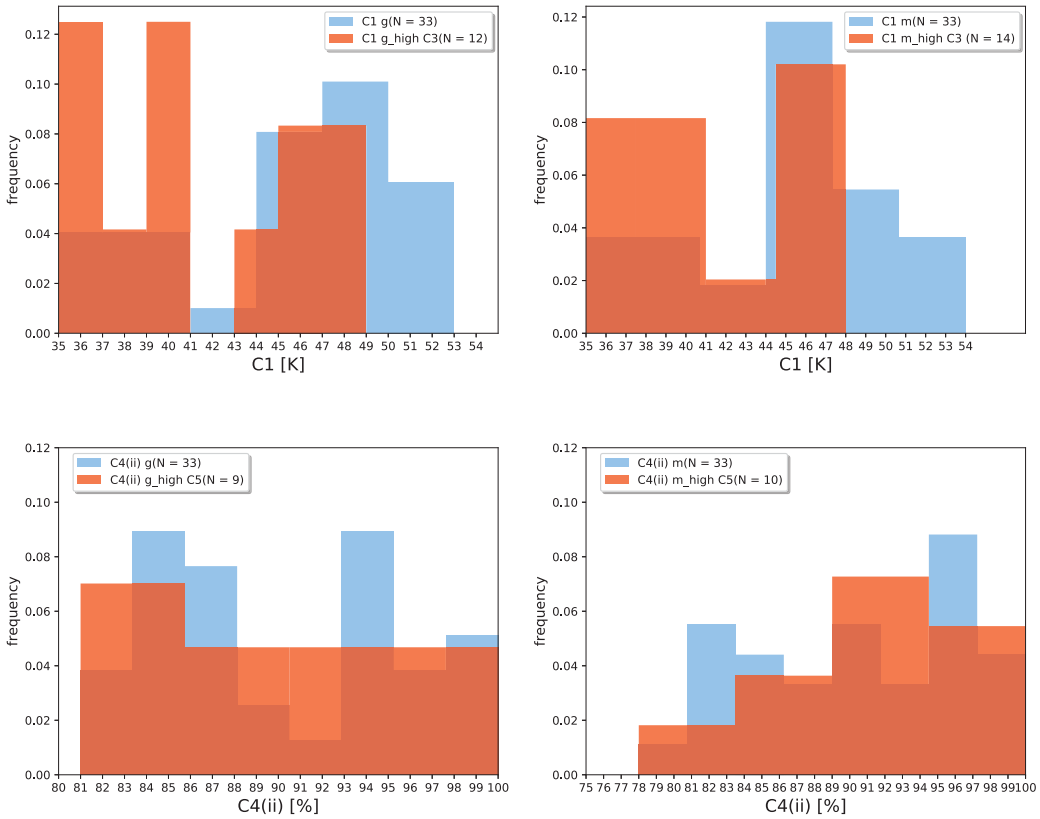

Fig. 4. Frequency of occurrence of condition C1 for all 33 cases (blue) and for cases with C3 above mean 75 percentile value of ASRv2 (orange) at genesis (g) (upper left) and maturity (m) (upper right) stages. Similar is shown for conditions C4(ii) with high C5 (above threshold) (bottom).

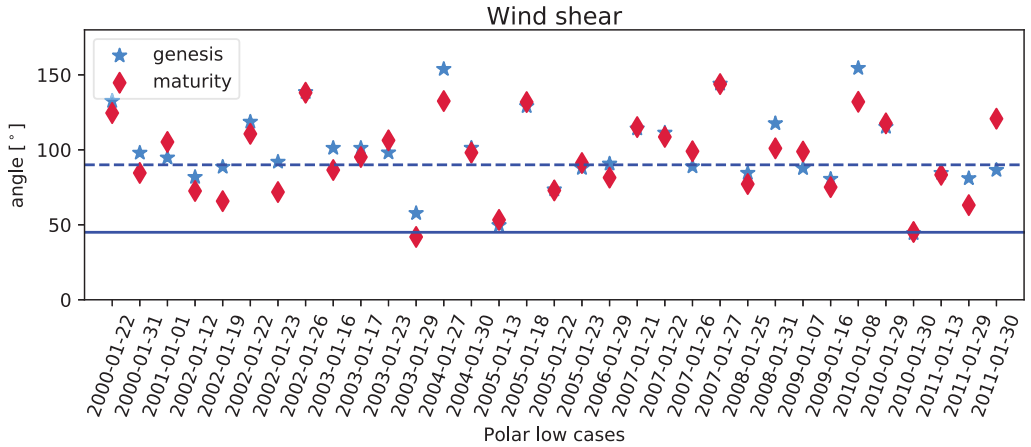

Fig. 5. Wind shear at genesis (blue stars) and maturity (red diamonds) stages. Blue lines separate forward (below blue thick line; 45°) and reverse (above blue dashed line; 90°) shear.

2.4. *Conditions for PL development*

In the literature, different conditions were used to identify and characterize PLs. These are listed below while often found values are given in Table 1.

i. **Condition 1: SST – T(500 hPa)**
From the thermal instability theory, which tried to explain the formation of PL through the instability inside of a CAO flowing over warmer sea, follows

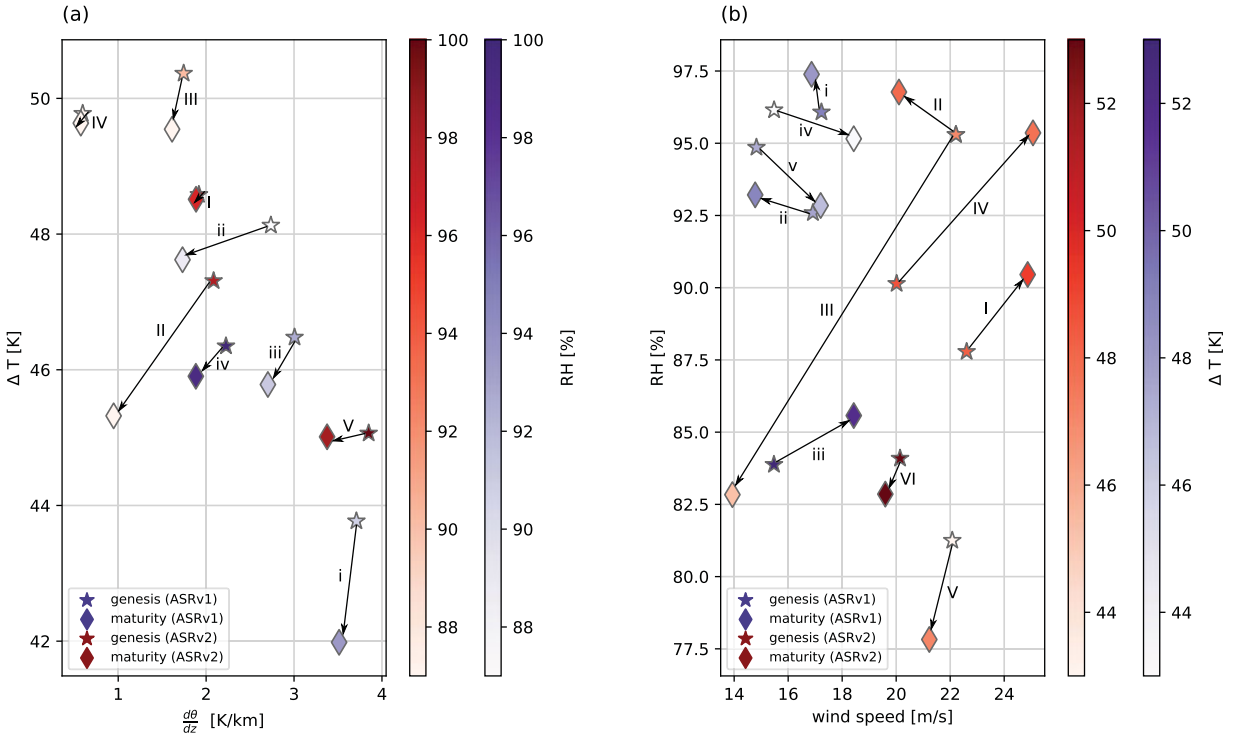

Fig. 6. (a) Mean 75 percentile values of C3: $\frac{d\theta}{dz}$ (*x*-axis), C1: ΔT (*y*-axis) and C4(ii): RH(850–950 hPa) (colour shading) for 4 cases of the ASRv1 (1 January 2001, 23 January 2005, 25 January 2008 and 29 January 2010) (purple) at genesis (stars) and maturity (diamonds) stages and 5 cases of the ASRv2 (26 January 2002, 17 January 2003, 21 January 2007, 7 January 2009 and 29 January 2011) (red). Lower (upper) case roman numbers above arrows indicate the same case at different stages from ASRv1 (ASRv2). (b) C5: near-surface wind speed (*x*-axis), C4(ii): RH(850–950 hPa) (*y*-axis) and C1: ΔT (color shading) for cases with strong C5 in ASRv1 (26 January 2002, 22 January 2005, 31 January 2008, 7 January 2009 and 30 January 2010) (purple) and ASRv2 (22 January 2002, 16 January 2003, 17 January 2003, 23 January 2005, 26 January 2007 and 27 January 2007) (red).

the logic of looking at the difference between the sea surface temperature (SST) and temperature at 500 hPa (T(500 hPa)). This temperature difference gives information on the static stability and is the most frequently used parameter for PL development and tracking (Noer and Ovhed, 2003; Zahn and von Storch, 2008).

A common threshold is $\geq$ 43 K, but some studies argue that, in choosing a strict threshold, some PL with lower SST-T(500 hPa) values (e.g. 36 K) can be missed (Blechschmidt et al., 2009; Terpstra et al., 2016). Nonetheless, we chose the stricter criteria of 43 K since the likelihood of a strong cyclone to be identified as a PL was reduced.

ii. **Condition 2: SST – T(2m)**

From WISHE theory, a PL is intensified by air–sea instability interaction as the PL is sustained by latent and sensible heat from the ocean, which are enhanced by wind. Seatra et al. (2008) and Linders et al. (2011) showed that strong winds can mix the subsurface sea water and increase the SST up to 3°C, which then feeds back to the PL itself and intensifies it. This means that for a higher difference between SST and temperature at 2 m height, greater thermal instability and more sensible heat at the lowest parts will be present which provide a favourable environment for PL formation. Therefore, in addition to checking for the wind threshold, SST and the difference between SST and temperature at 2 m have been analyzed in more recent studies. For some cases, this difference can be as high as 6–7 K (Terpstra et al., 2016).

iii. **Condition 3: Potential temperature lapse rate (LR) below 850 hPa**

While Condition 1 gives the broad picture on static stability, Condition 3 investigates the potential for convection in the boundary layer, here defined as below 850 hPa. When the potential temperature θ is constant with height, i.e. LR $= d\theta/dz$ is zero, dry adiabatic conditions indicating well-mixed conditions prevail. Any negative LR reveals absolute instability, which would quickly be removed by convection. Terpstra et al. (2016) could show that, for reverse shear PL, a strong boundary layer inversion between

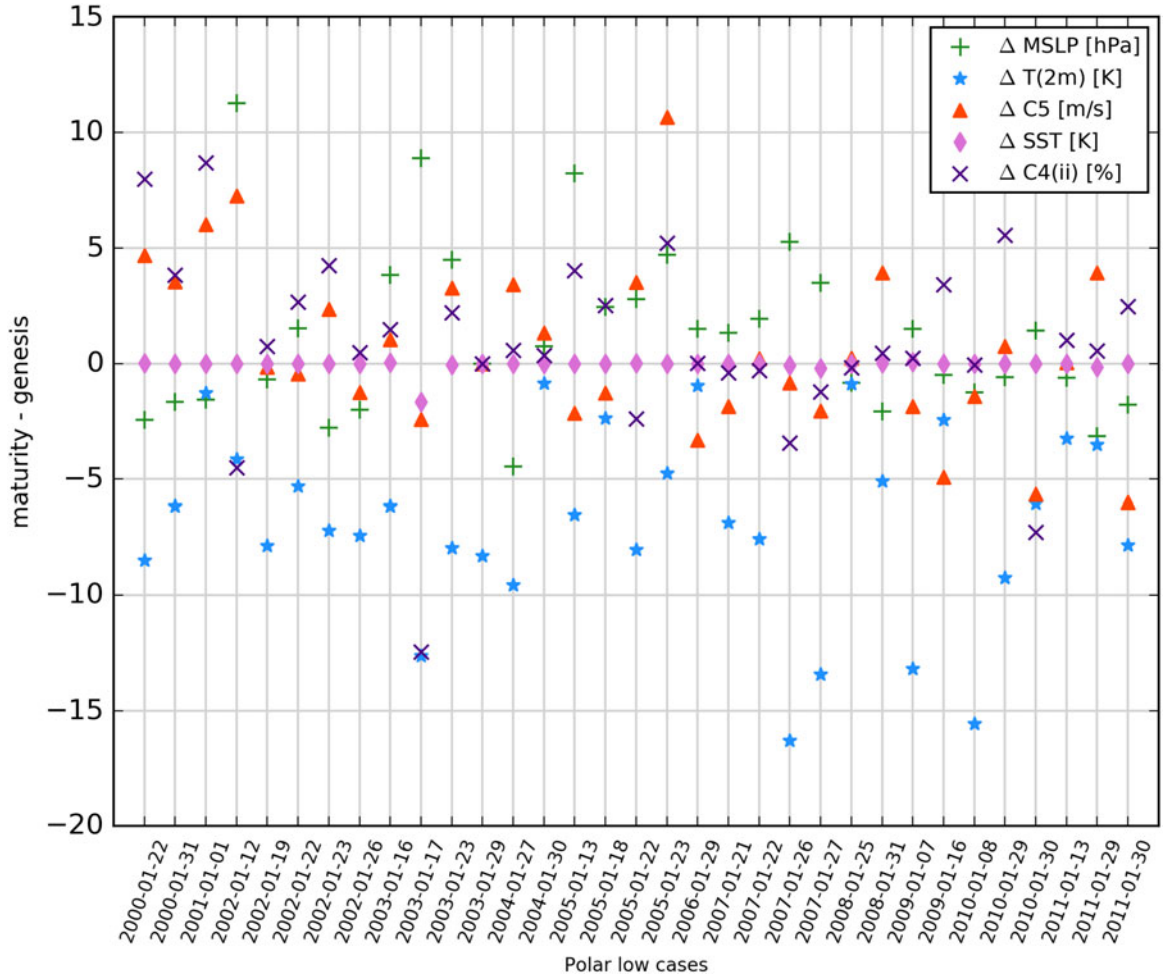

Fig. 7. Difference of environmental conditions between the genesis and the maturity stage. Shown are: MSLP difference (green pluses), temperature at 2 m (blue stars), near-surface wind speed (C5), SST, and RH in the layer between 850 and 950 hPa, C4(ii) (indigo crosses).

950 and 850 hPa occurs with LR increasing from slightly above zero in the lowest part of the boundary layer to roughly moist adiabatic conditions (LR about 3 K/km) in the free troposphere.

iv. **Condition 4 (i): RH(surface – 950 hPa) and (ii): RH(950–850 hPa)**
Since a PL gains its energy and continues its growth largely from the latent heat release, and therefore rapidly decays once over land, humidity is among the most important factors for PL formation and development. This is most prominent for the type C cyclones whose cyclogenetic dynamic is dominated by the action of strong mid-level latent heating (Plant et al., 2003). High amount of moisture and therefore more latent heat act as a substitute for smaller low-level temperature gradients (Bracegirdle and Gray, 2008). The more moisture a PL acquires during its growth, the more energy is available to continue intensification. Therefore, RH is another important parameter. Terpstra et al. (2016) found values of ~ 75% for C4(i) and ~ 82% for C4(ii).

v. **Condition 5: Near surface wind speed (NSWS)**
Probably one of the most notable features of a PL is the strong near-surface wind (can be above 25 m/s) with a threshold often used in the literature of at least 15 m/s (Rasmussen and Turner, 2003). Strong NSWS enhances turbulent fluxes from the sea surface into the atmosphere. Updrafts in the boundary layer transport moisture into colder environment in which moisture starts to condense releasing energy in the form of latent heat, important for PL development. Aside from this, NSWS is usually used to determine the intensity of a storm. It is well documented that PLs are warm core mesocyclones and therefore have reverse wind shears (Rasmussen and Turner 2003; Kolstad, 2006).

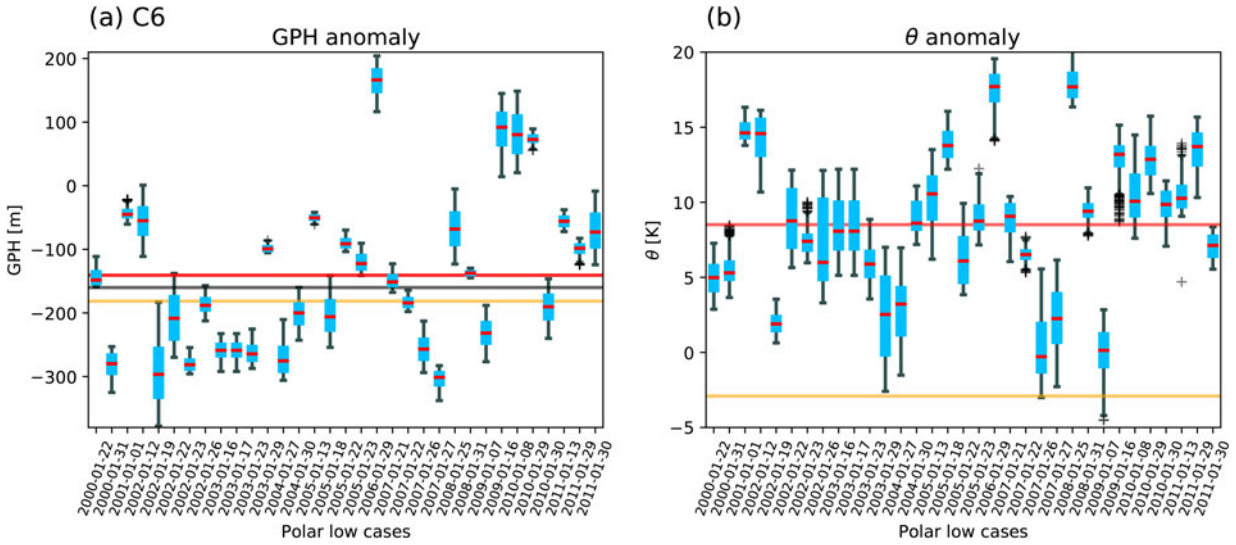

Fig. 8. Box plots for ASRv2 grid points within a 200 km radius around the genesis point for each of the January cases between 2000 and 2011. Anomaly of the GPH at the 500 hPa level (a) and potential temperature at the 850 hPa level (b). Lines correspond to those in Fig. 3. Blue boxes indicate interquartile range (IQR) and black whiskers the 1.5IQR. Individual outliers are presented as the black crosses.

However, according to the CISK theory, during its genesis stage when growth of an initial disturbance starts from interaction of small-scale organized convective cells with large-scale circulation, a PL can have a forward shear and a cold core (resemblance to extratropical cyclones). This kind of pre-PL environment was studied in Terpstra et al. (2016), and a method for calculation of a shear is presented below.

To calculate wind shear requires taking the angle between the mean and thermal wind flows (Duncan, 1978; Forbes and Lottes, 1985; Kolstad, 2006; Terpstra et al., 2016). The wind is said to have a reverse shear if the baroclinic waves propagate in the opposite direction to the thermal wind and a forward shear if propagation of baroclinic waves is in the direction of the thermal wind. The angle is calculated between 925 and 700 hPa using

$$\alpha = -\frac{1}{f}\left(\frac{\mathbf{v_T}\cdot\bar{\mathbf{v}}}{||\mathbf{v_T}||||\bar{\mathbf{v}}||}\right), \tag{1}$$

where

$$\mathbf{v_T} = \left(-\frac{1}{f}\frac{\partial(\phi_{700}-\phi_{925})}{a\partial\varphi}, \frac{1}{f}\frac{\partial(\phi_{700}-\phi_{925})}{a\cos\varphi\partial\lambda}\right) \tag{2}$$

and

$$\bar{\mathbf{v}} = \left(-\frac{1}{2f}\left(\frac{\partial\phi_{700}}{a\partial\varphi}+\frac{\partial\phi_{925}}{a\partial\varphi}\right), \frac{1}{2f}\left(\frac{\partial\phi_{700}}{a\cos\varphi\partial\lambda}+\frac{\partial\phi_{920}}{a\cos\varphi\partial\lambda}\right)\right), \tag{3}$$

are thermal and mean vertically averaged wind components, and ϕ_{700} and ϕ_{925} represent the geopotential at the 700 and 925 hPa levels, respectively. f denotes the Coriolis parameter, a the Earth's radius, φ the latitude and λ the longitude.

The angle is calculated for each grid cell in the radius of 200 km and then averaged to find the mean shear during the PL genesis stage. Using the α angle from above, it is possible to clearly distinguish between two types of the shear where the flow is said to be reverse if the angle is between $135^\circ \leq \alpha \leq 180^\circ$ and foreward if the angle is between $0^\circ \leq \alpha \leq 45^\circ$. For details, see Kolstad (2006).

vi. **Condition 6: Geopotential height (GPH) anomaly at 500 hPa**

A PL is usually well embedded into a CAO with a cold air mass flowing from the sea ice toward the warmer open ocean. A trough in the GPH field at the 500 hPa level indicates a cold air mass flow. Thus, during a PL, a 500 hPa GPH value is found to be lower than the climatological mean Blechschmidt et al. (2009). In the study by Forbes and Lottes (1985), where mesoscale vortices were investigated from December 1981 to January 1982, the mean GPH anomaly was negative and close to 160 m. That is the value taken here.

Hereinafter, instead of using the long names of the conditions outside of this section, we refer to C1, C2, and so on up to C6. Because MSLP is another parameter often used for PL and cyclone tracking and detection (Zahn and von Storch, 2008; Stoll et al., 2018), we inspected, in addition to the six conditions mentioned above, the mean

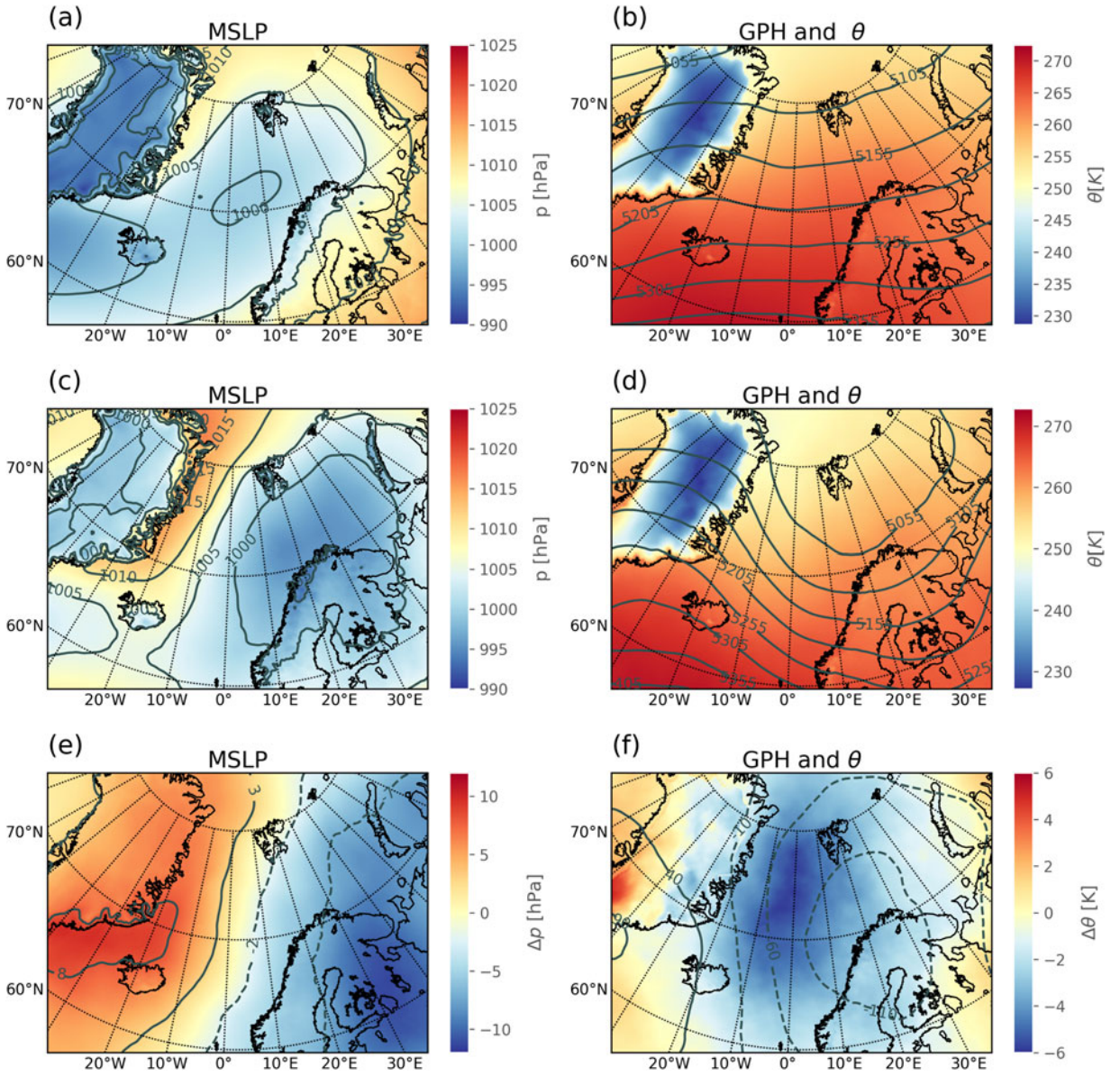

Fig. 9. Climatology of: (a) all 372 January days for MSLP (colour shading and grey-labeled counters, every 5 hPa) and (b) GPH at 500 hPa (grey-labeled contours, every 50 gpm) and potential temperature at 850 hPa (colour shading); (middle) As in the first row but for PL dates; (bottom) anomalies for both, MSLP (grey-labeled contours, every 5 hPa) (e) and GPH at the 500 hPa level (grey-labeled contours, every 50 gpm) and potential temperature (colour shading) (f).

sea-level pressure difference between the genesis and maturity stage.

3. PL environment

The results of the 33 January PL cases are presented in the following three subsections with the investigated criteria as listed in Table 1. We discuss those based on ASRv2 and include the comparison with ASRv1. First, we present the behaviour of conditions at the genesis stage and compare them with the mature stage. Second, we analyze the large-scale environments at the genesis stage and compare them with 12 years of January climatology.

3.1. Genesis stage

Figure 3 (upper left) shows the SST - T(500 hPa), C1, at the genesis(maturity) stage for all 33 cases. Each bar contains 75 percentile value derived from all the pixels values

of 200 km radius around the genesis(maturity) space-time point. Due to the inherent uncertainty in the ASR's positioning of the PLs (Fig. 2), the 75 percentile value provides more robust results. The results presented below are based on the ASRv2 while ASRv1 is used to compare PLs' representatives between the two ASR versions. More detailed figures with whisker plots for each stage separately are shown in the supplement. The results show that the mean value of C1 for nine cases did not reach the 43 K temperature difference threshold. However, the mean 75 percentile value for all cases was 45 K ± 5 K, which is 2 K above the threshold. Five cases, namely 23 January 2002, 23 January 2003, 27 January 2004, 21 January 2007 and 27 January 2007 had especially high C1, being above 50 K. By comparison, those cases show weaker lapse rates (cf. C3; Fig. 3). The region over which these kinds of PLs mostly occur was found to be east of 8°E and north of 70°N (Table 2).

Generally, it seems that, whenever a strong C1 (above ASRv2 mean) was present (55% of the cases), C3 was almost always below the mean, indicating that temperature instability (C1) acted as the main forcing mechanism for PL growth (Fig. 4). Similarly, when a weak C1 was present (27% of the cases), C3 often times was above the mean, showing that convection acted as the main triggering mechanism for PL growth (Fig. 4). The cases with strong C3, above 3 K/km, were forming mostly over the Barents Sea, with one case forming far east in the south western part of the Kara Sea in close proximity to Novaya Zemlya (Table 2).

The comparison between ASRv1 and ASRv2 shows smaller values of C1 in ASRv2 due to higher values of SST but the high standard deviation let the statistical significance unclear. Besides higher resolution, this difference could also be attributed to updated WRF's physics, which includes sub-grid scale cloud fraction interaction with the radiation and more accurate data assimilation (Bromwich et al., 2017).

The lowest part of the boundary layer shows that the mean values of the 75 percentile of the SST-T(2m) difference, C2, was 8.2 K with a standard deviation (STD) of 4.5 K. The majority of the cases reached the threshold of 6 K (ASRv1) or 8 K (ASRv2) (Table 1), with a few cases showing values above 15 K (Fig. 3). The cases with the highest values were mostly forming closer to the sea ice border, where the difference between the near-surface temperature and SST is larger. The cases with higher C2 appear to prefer the region between ~ 70° and 81°N (Table 2). Since the near surface cold air had time to warm up while flowing towards the south, C2 for other cases is lower.

For humidity at lower levels, RH ranged from ~ 81% below 950 hPa, C4 (i), to slightly above 80% between 850 hPa and 950 hPa, C4 (ii) (Fig. 3). In comparison to ASRv1, ASRv2 (Supplementary Figure S2) had an increase in RH for C4(i). However, at a higher level, there were only minor differences between the ASR versions in C4(ii).

A near-surface wind speed, C5 (Fig. 3), was below the 15 m/s threshold while the mean 75 percentile value was ~ 18 m/s with a STD of 3 m/s. For only 7 out of the 33 cases, maximum wind speed did not reach the 15 m/s threshold (Table 2). In comparison to ASRv1, there was a notable increase in the value of the considered condition (Supplementary Figure S3). With regard to the wind shear, January PLs seem to prefer reverse shear for their development, with only one case forming in the forward shear (Fig. 5).

3.2. Comparison of genesis and maturity stages

In this section, we compare conditions (explained in Section 2.4) at two different stages to find out which one (or the combination of) was contributing to the PL's persistence.

The maturity stage of the C1 condition in Fig. 3 is derived using the same radius as in the genesis stage but at the time of maturity. With a 75 percentile of 44.8 K, C1 was slightly lower than at the genesis stage. Moreover, its STD of 5.1 K was higher, and the same nine cases that did not reach the threshold of 43 K at the genesis stage did not reach it at the maturity stage either. For C1 at maturity stage, a greater difference between the two versions of reanalysis was detected. In ASRv1, the 75 percentile of C1 was 46.6 ± 2.8 K (which was slightly higher than at the genesis stage and with only 2 cases below the 43 K threshold).

Referring to the theory where C1 and C3 (Fig. 3) conditions relate to baroclinic instability and CISK, we checked for the change in these conditions to find out which of these conditions contributed to PL persistence from genesis to maturity. Looking at these two conditions, namely C1 and C3, we note similar behaviour at the genesis and maturity stages: Low C1 values (below threshold) are compensated with strong C3 (above threshold) (Fig. 4).

However, Fig. 3 shows that almost two-thirds of the cases had weaker vertical stability, C3, during the genesis stage than in the maturity stage. Twelve of those cases showed an increase in wind speed at maturity stage, which may indicate that this C5 condition is important for PL persistence. Five cases continued to persist and showed an increase in either C1 or C2, i.e. decreasing thermal stability at maturity stage. The remaining two cases had no increase in any of the conditions that promote PL strengthening or development, namely

conditions between C1 and C5 or decrease in C6. For the PLs with stronger C3 during the genesis stage, eight of the cases showed an increase in C1 while the remaining five even showed a decrease in terms of both C1 and C3. For those five, it was noted that RH was almost always above 90% (Fig. 6(a)) which may suggest that their persistence was triggered by energy gained through moisture.

Moreover, for the majority of intense PLs, in terms of near-surface wind speed, C5, the C4 (ii) was often above 90% (Fig. 3), meaning that latent heat release was important as a driving mechanism for those PLs. Cases that resolve this relation is represented in Fig. 6(b). Compared to ASRv1, ASRv2 shows higher values of C5, being above 20 m/s for those cases.

For the C2 condition, the mean value of the 75 percentile was the same as at the genesis stage, 6.4 K, with a STD of 3.4 K. C2 shows no significant positive correlation with any other condition. Nonetheless, a negative correlation of 0.6 was found with C4(ii) at both stages (not shown). Linders et al. (2011) have shown that a higher SST produces slightly more intense cyclones in terms of azimuthal wind speed and deeper sea-level pressure depression. However, our inspection of differences in the 75 percentile values between the genesis and maturity stages did not reveal a direct connection between SST and wind speed. Two cases with especially high values of C4 (ii) during the genesis stage showed a direct effect on an increased PLs intensity, in terms of the maximum wind speed at maturity stage (12 January 2002 and 22 January 2005). Those cases seemed to use energy stored in moisture. Moreover, increase in wind speed at the maturity stage was also found for the cases that also showed an increase in C4 (ii) (Fig. 4). Those cases intensified in wind speed by gaining energy from other sources.

Nonetheless, it seems that the change in temperature at 2 m is a better indicator of the change in wind speed intensity in general than it is the SST change (Fig. 7). The reason for this could be the faster variability of the temperature at 2 m, which is atmospheric component, compared to the SST which at maturity stage, did not increased more than 0.2 K. This explanation is reasonable since water warms much slower than air. Furthermore, it was also noted that temperature at 2 m always decreased at the maturity stage. Data from the STARS data base also showed that, generally, the cases with higher C4 (ii) were more persistent and lasted more than 13 h. Moreover, it seems that the near-surface humidity, C4 (i), behaves similarly to that of C4 (ii) (not shown).

To investigate pressure, we calculated the MSLP difference between the genesis and maturity stages. The results for that calculation show that the MSLP acts opposite to C4 (ii) during genesis and maturity stage. For majority of the cases that had lower pressure during the maturity stage, C4 (ii) was found to be higher during the genesis stage (Fig. 7). Generally, the opposite also holds true: if C4 (ii) was lower during the genesis stage, the MSLP was higher at the maturity stage. Although the correlation between these two conditions was negative, its strength of only 0.2 was too small to be significant.

To check for the difference between the climatology and the PL events, we calculated the 500 hPa GPH anomalies, C6. Those ranged from −400 to 200 gpm, with a mean value of ∼ 154 gpm below the climatological mean (Fig. 8(a)). This value is close to mean value found in Forbes and Lottes (1985), where GPH anomaly was 160 gpm. Nonetheless, one should compare values found in this study to those from Forbes and Lottes (1985) with caution since the period of investigation in that study was only one month.

Moreover, a comparison between ASRv1 and ASRv2 reveals a notable difference for this condition. While ASRv1 shows a mean value of −182 gpm, which is below that cited in the literature, ASRv2's mean value of −140 gpm is slightly higher and therefore above that of the threshold cited in the literature. Furthermore, the most striking difference between the two ASR versions is evident in the potential temperature, θ, anomaly at 850 hPa, where the mean value in ASRv1 is −3 K and in ASRv2 is ∼ 8 K.

3.3. Genesis environmental conditions compared to climatology

To obtain a better understanding of the PL environment, we looked at the spatial patterns of MSLP, GPH at 500 hPa and θ at 850 hPa and therefore show their composites at the genesis stage as a mean of all the PL cases and compare them to the January climatology.

The comparison between the PL composites and the January climatology of the MSLP shows that, generally, a central pressure depression is present at the border between the Norwegian and Greenland seas, while, during the PL events, it shifts towards the Norwegian coast (Fig. 9(a,c)). A deeper investigation of the anomaly shows that, during the PL events, the MSLP establishes a sharp boundary close to the 0° meridian and follows the Norwegian coast, touching the tip of the eastern part of Svalbard (Fig. 9(e)).

The previously discussed lower anomalous GPH for 54% of the cases found in our study compared to Forbes and Lottes (1985) seems to be explained by troughs of GPH that extend further south and are deeper for those cases. Fig. 9(d) shows that the trough in GPH at 500 hPa during the PL dates extends to the southern part of Norway.

The potential temperature anomaly can be as low as −6 K (Fig. 9) (f). This difference is slightly more pronounced between the northwestern side of the Norway and Svalbard. The analysis of C1 and C6 together brought to light that the cases with smaller C1 values have higher values of the GPH anomaly, indicating that the troughs were shallower and therefore temperature instability was also smaller. The summary of the results discussed above can be found in Table 2.

4. Summary and conclusions

In this study, we have used the ASR reanalyses to systematically investigate a set of often used criteria for PL detection and thus to identify the most important one(s) or the most important combination (Table 1). Since January is generally the month with the highest frequency of PLs, we chose that month for investigation. In total 33 cases were reported (Noer and Lien, 2010). PLs were studied within a radius of 200 km around the genesis point since Condron et al. (2006) found that only 2% of the polar mesocyclones identified on satellite imagery have a diameter lower than that value.

First, we analyzed the C1 condition and the mean ASRv2 value of 45 K was found to be 2 K higher than the commonly reported threshold discussed, e.g. in Terpstra et al. (2016). They noted that, for PLs forming in forward shear, a C1 threshold of 43 K was not reached. However, in our study, using only January PLs, we found only one case that developed in forward shear. This case had a C1 of 45 K. Moreover, lower C1 values, at least for January cases, do not have to be characteristic of PL forming in forward shear since nine of the cases that did not reach the C1 threshold were forming mostly in reverse shear. Therefore, it would be of interest to compare this finding with the other months of the PL season in a future analysis. Another reason for a higher C1 value could arise from our application of the ASR reanalysis, which has better resolution and uses a polar-optimized version of WRF, compared to ERA-I, which was used in the earlier study.

Nonetheless, in a few (seven) cases, PLs formed with C1 below 40 K. Since these cases with unfulfilled C1 condition have also been reported as PLs, we checked the combination of C1 with other conditions. We found that the majority of those cases fulfilled the C3 condition (even commonly showed stronger lapse rates) indicating that convection was probably the key driving mechanism for their growth.

The analysis of the area of origin showed that the cases with especially high values of C1 formed mostly east of 8°E and north of 70°N while the cases with stronger C3 originated mostly over the Barents Sea.

Analysing C2, we noted that the PLs with extremely high values were forming closer to the sea-ice edge, where the temperature difference between the warmer open ocean and the near-surface air advected from the ice was much higher. The PL cases with higher C2 values prefer a more eastern region for their development, between 10° and 28°E and 70 and 81°N. It was also found that PL cases that possessed higher values of C4 (ii), and therefore had more latent heat energy available for their growth, had a more direct connection to the wind speed intensity at the mature stage than the SST, which at the maturity stage had rarely increased more than 0.2 K. This result differs from the one found in Linders et al. (2011), where a non-hydrostatic numerical model showed that an increase in SST promotes slightly stronger winds and deeper sea-level pressure of a PL.

The analysis of the MSLP in combination with C4 (ii) at the two different stages of PL development showed that these two variables have opposite behaviour. This difference means that, at the genesis stage, when the MSLP is higher, C4 (ii) is lower, and vice versa.

While analyzing the GPH anomalies, we found a larger difference between the two ASR versions, where ASRv1 (ASRv2) showed values that were lower (higher) than those in a previous study (Forbes and Lottes, 1985). However, both versions showed that the minimum value can be lower than −400 gpm.

Furthermore, for PLs with a lower C1, we found that C6 values were greater than the threshold reported in the literature. This means that, for these cases, cold air masses were shallower and therefore the temperature instability was weaker.

The investigation into the climatology of MSLP, potential temperature fields (850 hPa) and GPH (500 hPa) revealed that the MSLP field shows a central low over the region between the Norwegian and Greenland seas while, during the PL dates, this central low was shifted over the northeastern part of the coastal Norway. Here, no significant difference between the two versions of ASR was found.

Overall, the results of this study indicate that there is not one condition that is the most relevant for PL formation or growth. It seems that more information on PL behaviour at the maturity stage can be gained by a combination of conditions. For a few cases, higher amounts of RH at the genesis stage appear to be able to produce more intense PLs at the maturity stage. Therefore, it would be of relevance to investigate this relationship more deeply in the future. For our concerted analysis of environmental PL conditions, we limited our study to PLs in January, the month with highest PL occurrence and the coldest month of the PL season (October–May). We are aware that this leaves us with a limited number of cases, namely 33 PL

cases in total, which limits the significance of our statements. However, we confirm that the differences between the two ASR versions are robust for all conditions (C1–C5). Therefore, a possible next step would be to analyze the whole PL season. Another interesting future study could be the analysis of PL formation and development under various climate change conditions.

Supplementary data

Supplemental data for this article can be accessed here.

Acknowledgements

We are thankful to Polar Meteorology Group at Byrd Polar and Climate Research Center, the Ohio State University, for production of ASR that can be downloaded from https://rda.ucar.edu/datasets/ds631.0/.

Funding

This research has been supported by the Deutsche Forschungsgemeinschaft (DFG, German Research Foundation) – Project number 268020496 – TRR 172, within the Transregional Collaborative Research Center 'ArctiC Amplification: Climate Relevant Atmospheric and SurfaCe Processes, and Feedback Mechanisms (AC)^3'.

References

Akperov, M, Rinke, A., Mokhov, I. I., Matthes, H., Semenov, V. A., Adakudlu, M., et al. 2018. Cyclone activity in the Arctic from an ensemble of regional climate models (Arctic CORDEX). *J. Geophys. Res. Atmos.* **123**, 2537–2554. doi:10.1002/2017JD027703

Blechschmidt, A.-M. 2008. A 2-year climatology of polar low events over the Nordic Seas from satellite remote sensing. *Geophys. Res. Lett.* **35**, L09815.

Blechschmidt, A. M., Bakan, S. and Graßl, H. 2009. Large-scale atmospheric circulation patterns during polar low events over the Nordic seas. *J. Geophys. Res.* **114**, D06115.

Bracegirdle, T. J. and Gray, S. L. 2008. An objective climatology of the dynamical forcing of a polar lows in the Nordic seas. *Int. J. Climatol.* **28**, 1903–1919. doi:10.1002/joc.1686

Bromwich, D. H., Hines, K. M. and Bai, L.-S. 2010. Development and testing of polar Weather Research and Forecasting Model: 2. Arctic Ocean. *J. Geophys. Res. Lett.* **114**, D08122.

Bromwich, D. H., Wilson, A. B., Bai, L.-S., Moore, G. W. K. and Bauer, P. 2016. A comparison of the regional Arctic System Reanalysis and the global ERA-Interim reanalysis for the arctic. *Qjr. Meteorol. Soc.* **142**, 644–658. doi:10.1002/qj.2527

Bromwich, D. H., Wilson, A. B., Bai, L., Liu, Z. and Barlage, M. 2018. The Arctic System Reanalysis Version 2. *Bull. Amer. Meteor. Soc.* **99**, 805–828. doi:10.1175/BAMS-D-16-0215.1

Carmack, E. C., Aagaard, K., Swift, J. H., MacDonald, R. W. and McLaughlin, F. A. 1997. Changes in the temperature and tracer distributions within the Arctic Ocean: results from the 1994 Arctic Ocean section. *Deep Sea Research II* **44**, 1487–1502. doi:10.1016/S0967-0645(97)00056-8

Charney, J. G. and Eliassen, A. 1964. On the growth of the hurricane depression. *J. Atmos. Sci* **21**, 68–75. doi:10.1175/1520-0469(1964)021<0068:OTGOTH>2.0.CO;2

Condron, A., Bigg, G. and Renfrew, I. A. 2006. Polar Mesoscale Cyclones in the Northeast Atlantic: Comparing Climatologies from ERA-40 and Satellite Imagery. *Monthly Wealth Rev.* **134**, 1518–1533. doi:10.1175/MWR3136.1

Condron, A. and Renfrew, I. A. 2013. The impact of polar mesoscale storms on northeast Atlantic Ocean circulation. *Nature Geosci.* **6**, 34–37. doi:10.1038/ngeo1661

Dannevig, P. 1954. : *Meteorologi for Flygere.* Aschehoug, Oslo.

Douglas, M. W., Shapiro, M. A., Fedor, L. S. and Saukkonen, L. 1995. Research aircraft observations of a polar low at the East Greenland ice edge. *Monthly Weather Rev.* **123**, 5–15. doi:10.1175/1520-0493(1995)123<0005:RAOOAP>2.0.CO;2

Duncan, C. 1978. Baroclinic instability in a reverse shear flow. *Meteor. Mag.* **107**, 17–23.

Emanuel, K. 1986. An air–sea interaction theory for tropical cyclones, part1: Steady-state maintenance. *J. Atmos. Sci.* **43**, 585–605. doi:10.1175/1520-0469(1986)043<0585:AASITF>2.0.CO;2

Emanuel, K. and Rotunno, R. 1989. Polar lows as Arctic hurricanes. *Tellus* **41A**, 1–17. doi:10.1111/j.1600-0870.1989.tb00362.x

Forbes, G. and Lottes, W. D. 1985. Classification of mesoscale vortices in polar airstreams and the influence of the large-scale environment on their evolutions. *Tellus* **37A**, 132–155. doi:10.1111/j.1600-0870.1985.tb00276.x

Føre, I., Kristjánsson, J. E., Saetra, Ø., Breivik, Ø., Røsting, B. and co-authors. 2011. The full life cycle of a polar low over the Norwegian Sea observed by three research aircraft flights. *Qjr. Meteorol. Soc.* **137**, 1659–1673. doi:10.1002/qj.825

Harley, D. G. 1960. Frontal contour analysis of a polar low. *Meteor. Mag* **89**, 146–147.

Harold, T. W. and Browning, K. A. 1969. The polar low as a baroclinic disturbance. *QJ. Royal Met. Soc.* **95**, 710–723. doi:10.1002/qj.49709540605

Kolstad, E. W. 2006. A new climatology of favourable conditions for reverse-shear polar lows. *Tellus* **58A**, 344–354.

Lind, S., Ingvaldsen, R. B. and Furevik, T. 2018. Arctic warming hotspot in the northern Barents Sea linked to declining sea-ice import. *Nat. Clim. Change* **8**, 634–639. doi:10.1038/s41558-018-0205-y

Linders, T., Saetra, Ø. and Bracegirdle, T. J. 2011. Limited polar lows sensitivity to sea-surface temperature. *Q. J. Res. Meteorol. Soc.* **137**, 58–69. doi:10.1002/qj.718

Michel, C., Terpstra, A. and Spengler, T. 2018. Polar Mesoscale Cyclone Climatology for the Nordic Seas Based on ERA-

Interim. *J. Climate* **31**, 2511–2532. doi:10.1175/JCLI-D-16-0890.1

Montgomery, M. T. and Farrell, B. 1992. Polar low dynamics. *J. Atmos. Sci.* **49**, 2482–2505.

Morison, J., Kwok, R., Peralta-Ferriz, C., Alkire, M., Rigor, I., Andersen, R. and Steele, M. 2012. Changing arctic ocean freshwater pathways. *Nature* **481**, 66–70. doi:10.1038/nature10705

Noer, G. and Lien, T. 2010. : Dates and positions of polar lows over the Nordic seas between 2000 and 2010. *Tech. Rep. met.no report 16/2010*, Norwegian Meteorological Institute, 16/2010. Online at: https://www.met.no/publikasjoner/met-report/met-report-2010.

Noer, G. and Ovhed, M. 2003. Forecasting of polar lows in the Norwegian and Barents Sea – proc. of the 9th meeting of the EGS Polar Lows Working Group, Cambridge, UK.

Noer, G., Saetra, Ø., Lien, T. and Gusdal, Y. 2011. A climatological study of polar lows in the Nordic Seas. *Qjr. Meteorol. Soc.* **137**, 1762–1772. doi:10.1002/qj.846

Plant, R. S., Craig, G. C. and Gray, S. L. 2003. On a threefold classication of extratropical cyclogenesis. *Qjr. Meteorol. Soc.* **129**, 2989–3012. doi:10.1256/qj.02.174

Rasmussen, E. 1979. The polar low as an extratropical CISK disturbance. *Quart. J. Roy. Meteor. Soc* **105**, 531–549. doi:10.1002/qj.49710544504

Rasmussen, E. A. and Turner, J. 2003. *Polar Lows*. Cambridge University Press, Cambridge, UK.

Sardie, J. M. and Warner, T. T. 1983. On the mechanisms for the development of polar lows. *J. Atmos. Sci.* **40**, 869–881. doi:10.1175/1520-0469(1983)040<0869:OTMFTD>2.0.CO;2

Ø. Saetra, Y., Gusdal, S., Eastwood, J., Debernard, P. E., Isachesen, H. and co-authors. 2010. Sea surface temperature and altimeter synergy for improved forecasting of polar lows (STARS). Scientific analysis plan (d3). *Tech. Rep.*, Norwegian Meteorological Institute, 49 pp. Online at: http://polarlow.met.no/stars/.

Seatra, O., Linders, T. and Debernard, J. 2008. Can polar lows lead to a warming of the ocean surface? *Tellus* **60**, 141–153. doi:10.1111/j.1600-0870.2007.00279.x

Serreze, M. C. and Francis, J. A. 2006. The arctic amplification debate. *Climate Change* **76**, 241–264. doi:10.1007/s10584-005-9017-y

Shapiro, M. A., Fedor, L. S. and Hampel, T. 1987. Research aircraft measurements of polar low over the Norwegain Sea. *Tellus* **39A**, 272–306. doi:10.1111/j.1600-0870.1987.tb00309.x

Smirnova, J. and Golubkin, P. 2017. Comparing polar lows in atmospheric reanalyses: Arctic System Reanalysis versus ERA-Interim. *Monthly Wealth Rev.* **145**, 2375–2383. doi:10.1175/MWR-D-16-0333.1

Stoll, P., Graversen, R. G., Noer, G. and Hodges, K. 2018. An objective global climatology of polar lows based on reanalysis data. *Q. J. R. Meteorol. Soc.* **144**, 2099–2117. doi:10.1002/qj.3309.

Terpstra, A., Michel, C. and Spengler, T. 2016. Forward and reverse shear environments during polar low genesis over the Northeast Atlantic. *Monthly Weath Rev.* **144**, 1341–1354. doi:10.1175/MWR-D-15-0314.1

Tilinina, N., Gulev, S. and Bromwich, D. H. 2014. New view of Arctic cyclone activity from the Arctic system reanalysis. *Geophys. Res. Lett.* **41**, 1766–1772. doi:10.1002/2013GL058924

Wendisch, M., et al. 2017. Understanding causes and effects of rapid warming in the arctic. EOS, 98. doi:10.1029/2017EO064803

Wilson, B. A., Bromwich, H. D. and Hines, K. M. 2011. Evaluation of polar WRF forecasts on the Arctic System Reanalysis domain: Surface and upper air analysis. *J. Geophys. Res. Lett* **116**, D11112. doi:10.1029/2010JD015013

Wilson, B. A., Bromwich, H. D. and Hines, K. M. 2012. Evaluation of polar WRF forecasts on the Arctic System Reanalysis domain: 2. Atmospheric hydrologic cycle. *J. Geophys. Res. Lett.* **117**, D04107.

Zabolotskikh, E. V., Gurvich, I. A. and Chapron, B. 2015. New areas of polar lows over the Arctic as a result of the decrease in sea ice extent. *Izv. Atmos. Ocean. Phys.* **51**, 1021–1033. doi:10.1134/S0001433815090200

Zahn, M. and von Storch, H. 2008. A long term climatology of North Atlantic polar lows. *Geophys. Res. Lett.* **35**, L22702. doi:10.1029/2008GL035769

Zappa, G., Shaffrey, L. and Hodges, K. 2014. Can polar lows be objectively identified and tracked in the ECMWF operational analysis and the ERA-Interim reanalysis? *Monthly Weath Rev.* **142**, 2596–2608. doi:10.1175/MWR-D-14-00064.1